Effect of an interlayer on the emission characteristics of a white-light-emitting electroluminescent device with a Pr and Ce doubly doped ZnS phosphor layer

Y. H. Lee,[a] B. K. Ju, M. H. Song, T. S. Hahn, and M. H. Oh
Division of Electronics and Information Technology, Korea Institute of Science and Technology, P.O. Box 131, Cheongryang, Seoul, Korea

D. H. Kim
Department of Physics, Yeungnam University, Kyungsan, Korea

(Received 10 November 1995; accepted for publication 26 February 1996)

We have investigated light-emission characteristics of a white-light-emitting electroluminescent device with a doubly doped ZnS:Pr,Ce,F phosphor layer. We found that optimum codoping of Ce enhances the emission characteristics compared to the electroluminescent device with a singly doped ZnS:Pr,F layer. We also found that introducing an additional thin-insulating Si_xN_y interlayer between the lower insulating layer and the phosphor layer significantly stabilizes the aging characteristics and improves the luminous efficiency. © *1996 American Institute of Physics.* [S0021-8979(96)04911-0]

I. INTRODUCTION

The ultimate goal of present color thin film electroluminescent (TFEL) devices is to realize bright blue emission. As is well known, one approach to achieve a full color electroluminescent (EL) device is to use a filter in front of a white-light-emitting device. Accordingly, it is desirable to prepare white-light-emitting TFEL devices with high intensity, especially with an intense enough blue component.

The luminescence of rare earth ions (Ce, Tb, Eu, Pr, Tm, etc.) embedded in the different host materials has been intensively investigated because of the important applications of these materials in lasers and display materials.[1] Pr ions are often used as white-light-emitting luminescent centers in ZnS and SrS host layers. However, the spectral components of singlely Pr-doped SrS or ZnS could not satisfy the required level needed for application to color EL devices.

In many works, the stacked insulating layers have been adopted in order to achieve reliable device performance with a long lifetime, but without significant changes in luminance or threshold voltages, etc. The insulating layer must satisfy all of the following requirements: it must have high charge storage capacity, self-healing breakdown, good adhesion to the phosphor layer, high photoetching resistivity, high moisture resistivity, and no pinhole defects. The insulating layers of commercialized EL devices consist of typical lower and upper dielectric layers with one or two interlayers inserted as a role for ion barriers or charge accelerating layer. Despite intensive studies on the stacked structure with interlayers, the role of the interlayer on the performance of an EL device has not yet been clarified.[2]

In this study, as an extension of our previous work on a SrS:Pr EL device,[3] we first report the optical, structural, and electrical characteristics of a newly developed Pr and Ce doubly doped ZnS EL device with improved luminance characteristics and chromaticity for white emission. Second, the transferred charge and light-emission characteristics with and without an interlayer between the lower insulating layer and the phosphor layer will be reported. The latter is important in order to clarify the role of an interlayer (or stacked insulators) in the EL emission process and degradation phenomena.

II. SPECIMEN PREPARATION

The schematic structure of our TFELD device fabricated in this study is shown in Fig. 1. A $BaTa_2O_6$ insulating layer, ZnS:Pr,Ce light-emitting layer, Si_xN_y insulating layer, and Al back electrode were sequentially deposited on Sn-doped In_2O_3(ITO) coated Corning 7059 glass substrate. The EL device with an additional interlayer consists of an extra thin layer of Si_xN_y between the lower $BaTa_2O_6$ layer and the phosphor layer.

The CeF_3 and PrF_3 powder for the light-emitting centers were purchased from Cerac Co. to prepare doubly doped

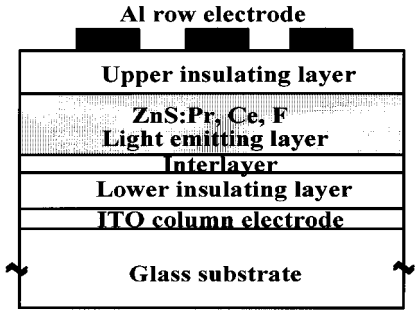

FIG. 1. The schematic structure of our thin film electroluminescent device.

[a]Electronic mail: lyh@kistmail.kist.re.kr

 0021-8979/96/79(11)/8717/8/$10.00

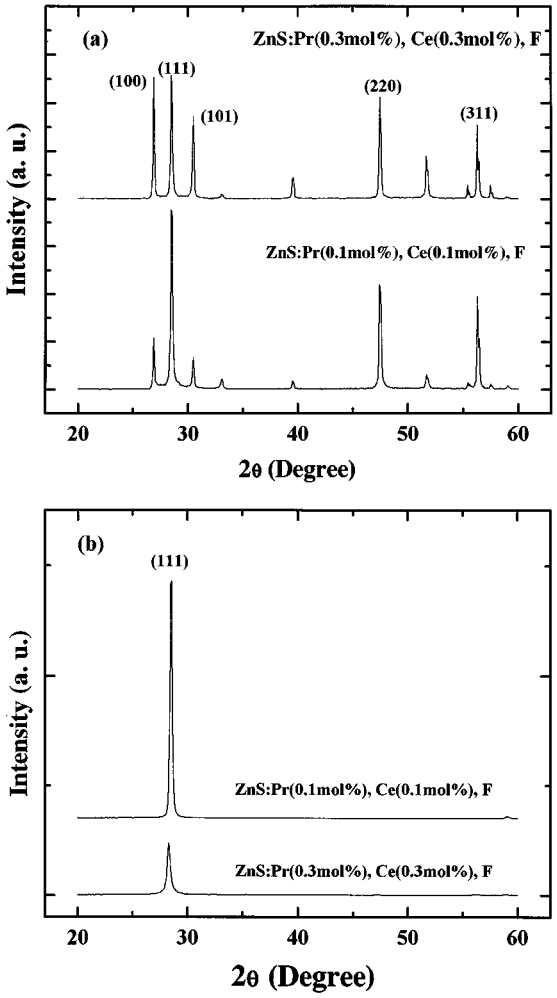

FIG. 2. X-ray diffraction patterns of (a) ZnS:Pr,Ce,F powder and (b) thin film for the two different Pr and Ce concentrations.

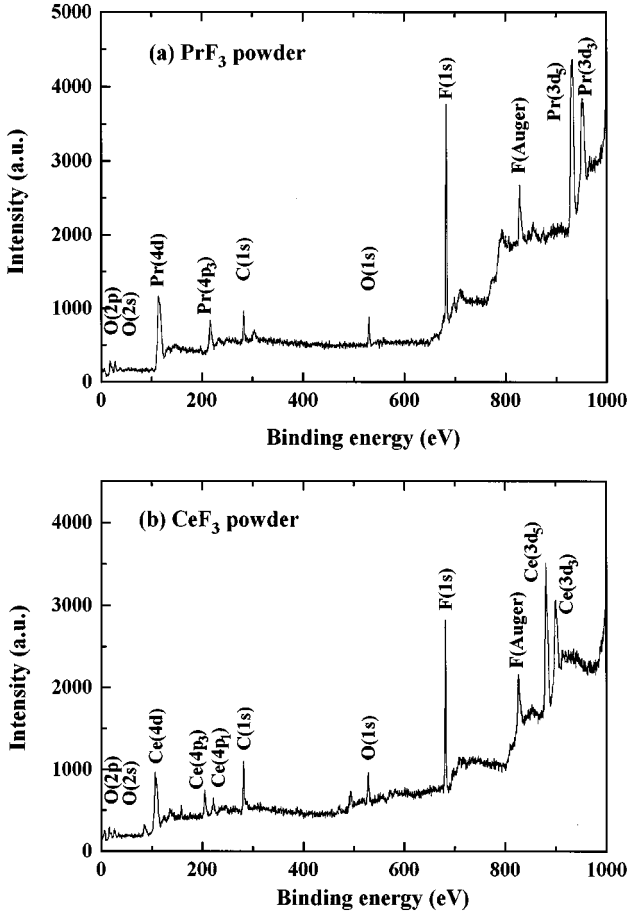

FIG. 3. X-ray photoelectron spectra (XPS) of (a) PrF_3 and (b) CeF_3.

ZnS:Pr(0.1 and 0.3 mol %) and Ce(0.1 and 0.3 mol %). A normal sequence of phosphor processes was employed and the firing was carried out in a N_2:H_2 (9:1) atmosphere. The ZnS:Pr,Ce,F layer was formed by electron-beam (EB) evaporation at approximately 2×10^{-5} Torr. After deposition of the phosphor layer, the sample was annealed at 400 °C for half an hour under the vacuum of 5×10^{-6} Torr. The $BaTa_2O_6$ insulating layer was deposited by rf magnetron sputtering at a working pressure of 5×10^{-3} Torr in a mixture of Ar and 20% of O_2 with a deposition rate of 2–3 nm/min using 4 in. hot-pressed ceramic targets. The Si_xN_y interlayer and the upper insulating layer were deposited at a substrate temperature of 120 °C in a mixture of Ar and 20% of N_2. The thickness of $BaTa_2O_6$, Si_3N_4 insulators and phosphor layers are 300, 150, and 1000 nm, respectively. The thickness of the interlayer was about 50 nm.

III. EXPERIMENTAL RESULTS AND DISCUSSION

A. Dependence of the optical characteristics of an EL device on emission centers

Figures 2(a) and 2(b) show the x-ray diffraction (XRD) results of ZnS:Pr,Ce,F powder and thin film for two different Pr and Ce concentrations, respectively. The cubic phase is dominant regardless of the dopant concentrations within our doping level. The chemical states of Pr, Ce, and F were studied by x-ray photoelectron spectroscopy. Figures 3(a) and 3(b) show the spectra of the PrF_3 and CeF_3 powders for reference. Figures 4(a) and 4(b) show a $2P^{3/2}$ spectrum of S^{2-} ions in ZnS layers doped with two different concentra-

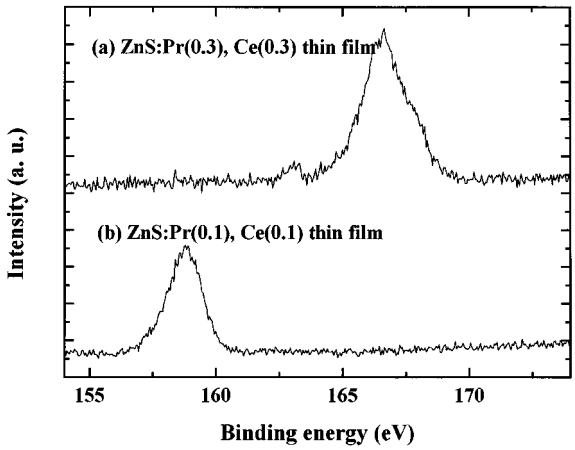

FIG. 4. XPS spectra of S_{2P}^{2-} of ions in an electron-beam evaporated ZnS thin layer doped with (a) Pr(0.1 mol %)/Ce(0.1 mol %) and (b) Pr(0.3 mol %) and Ce(0.3mol %).

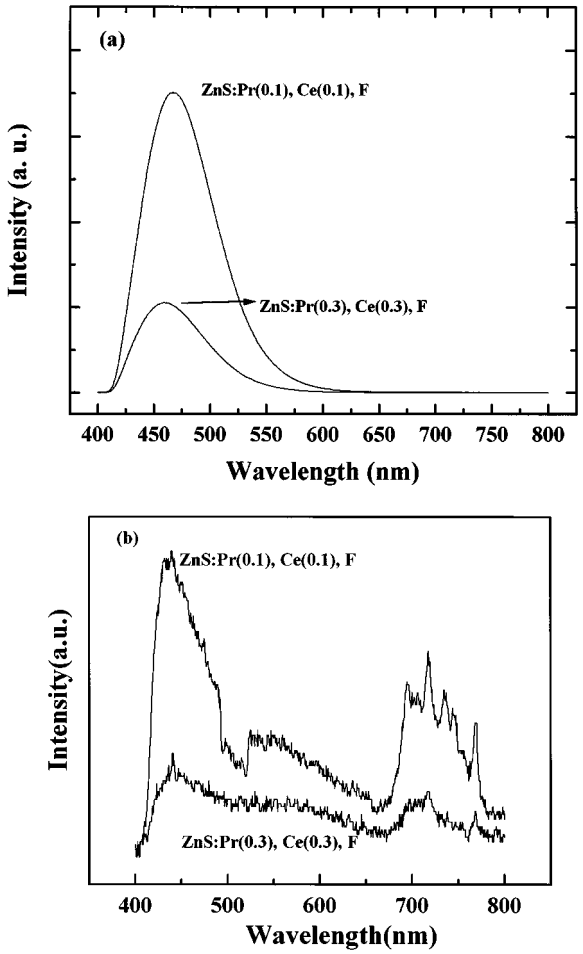

FIG. 5. Photoluminescence spectra of (a) ZnS:Pr, Ce, F powder and (b) a thin film layer.

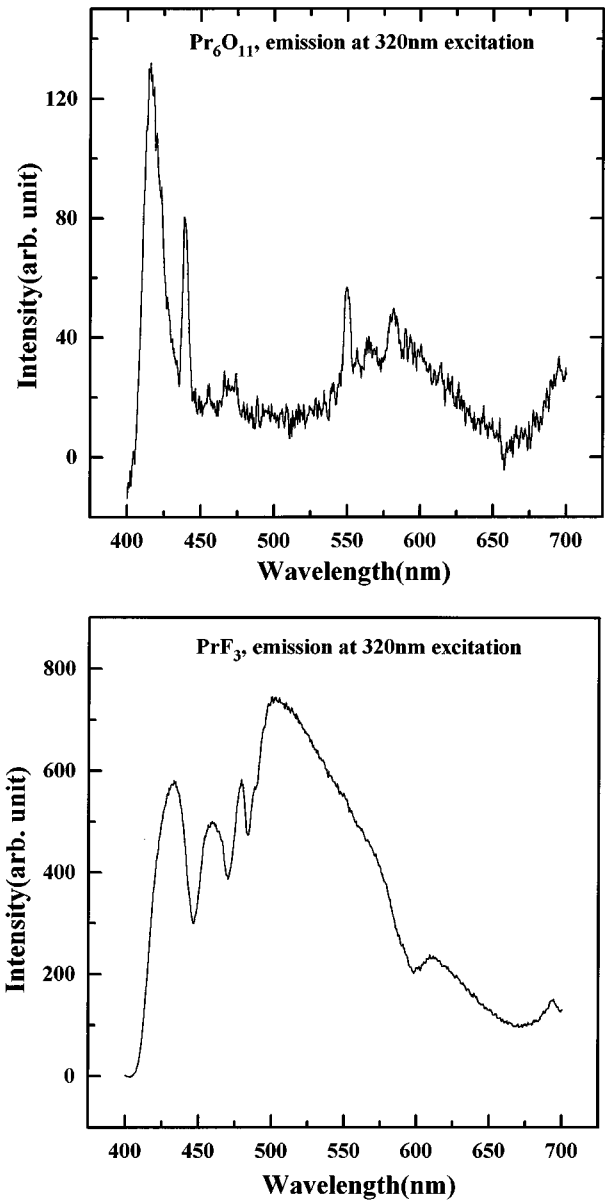

FIG. 6. Photoluminescence spectra of Pr_6O_{11} and PrF_3 powder.

tions of Pr and Ce. When the ZnS thin films are doped with 0.1 mol % of Pr and Ce, two peaks of S_{2p} (at about 157 eV) and S_{2p} (at about 159 eV) are combined. These arise from the S ion being bound to Zn to form the ZnS compound. On the other hand, Fig. 4(a) shows two peaks of S_{2p} at 166 and 167 eV, which arise from other states of S in 0.3 mol % of Pr- and Ce-doped ZnS and we attribute them to sulfate[4] SO_4^{2-} and/or SO_3^{2-}.

Figures 5(a) and 5(b) show the photoluminescence (PL) of the ZnS:Pr,Ce,F powder and thin film, respectively, for two different Pr and Ce concentrations. Unlike the typical narrow emission line of rare earth ions, the PL emission spectrum of ZnS:Pr,Ce,F exhibits a broad peak. The advanced analysis of the line shape of the powder phosphor fit into four components at about 495, 535, 550, and 607 nm. The 495 nm peak can be attributed to the transition of $^3P_0 \rightarrow {}^3H_4$. The 535 and 550 nm peaks can be attributed to the transition of $^3P_1 \rightarrow {}^3H_5$, and the 550 nm peak to the transition of $^3P_0 \rightarrow {}^3H_5$. The assignment of the 607 nm peak is not easy at the present time. The doping concentration dependence of the ZnS:Pr, Ce powder is observed for a peak position having a short wavelength.

Here, we present the PL spectra of Pr^{3+} in pure Pr_6O_{11} and PrF_3 powder in Fig. 6 in order to understand the possible origin of line broadening. The emission peaks of Pr_6O_{11} are different from those of PrF_3 considerably in linewidths. We can understand that those differences are due to the strong effect of the local crystal field on the energy level of Pr^{3+}. Figure 6 indicates that the Pr^{3+} ions in Pr_6O_{11} are all located at the same crystal field, thus exhibiting a narrowband feature, while the Pr^{3+} ions in PrF_3 occupy different positions.

The presence of concentration effects and the line broadening in the PL emission spectrum of ZnS:Pr,Ce,F powder can be seen as a consequence of the interaction between Pr^{3+} ions and Ce^{3+} occupying different sites in this host lattice, as shown in XRD results. The spectrum of the ZnS:Pr,Ce,F thin layer, in contrast to the powder results, which suggests that Pr and Ce ions in cubic phase dominant the ZnS layer easily occupied at more preferable sites, thus showing the distinct emission structure of Pr and Ce ions.

The EL spectra of ZnS:Pr,Ce,F TFEL devices at room temperature and 168 K, respectively, are shown in Figs. 7(a)

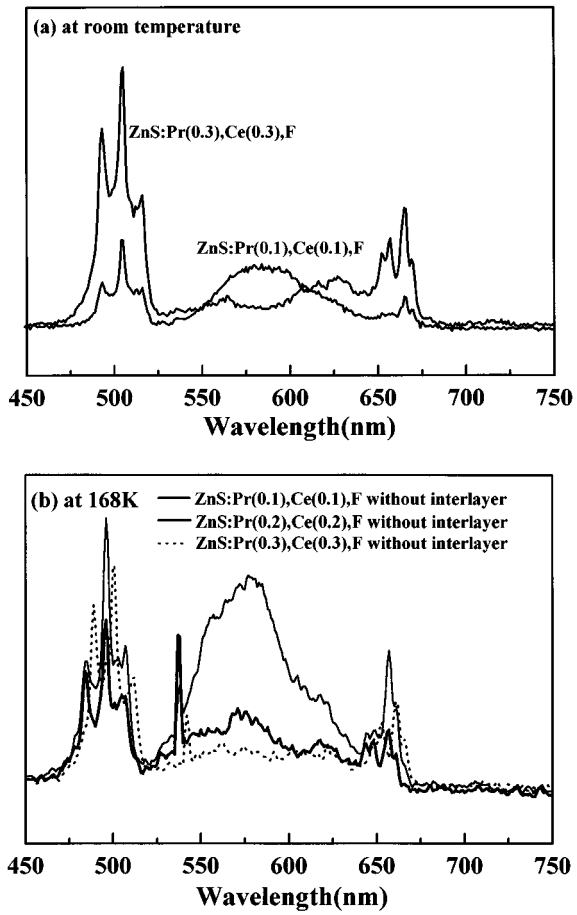

FIG. 7. Electroluminescence spectra of our ZnS:Pr, Ce, F electroluminescent devices.

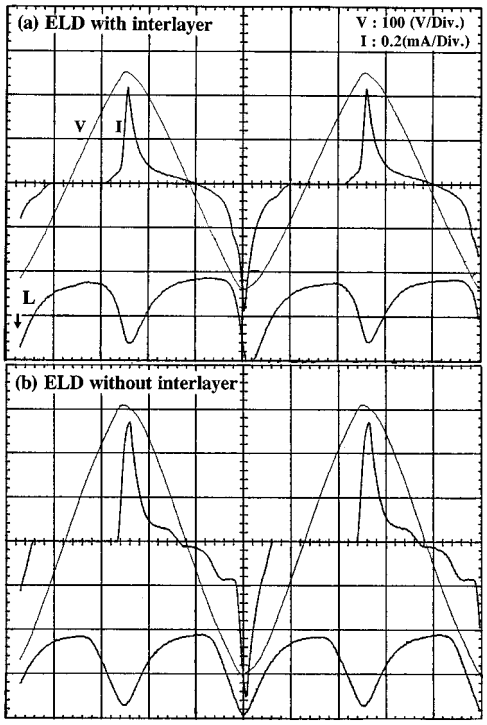

FIG. 8. The temporal response of current (I) and emission of EL devices (L) under high voltage excitation (V).

and 7(b). Figure 7(b) shows the EL emission spectrum of ZnS thin films doped with 0.1 mol % of Pr and Ce along with three distinct main peaks: one peak around 490 nm (blue–green) is due to $^3P_0-^3H_4$ transition of Pr^{3+} and the broad intense peaks of Ce and (or Pr) around 525–550 nm, and the 580 nm peak overlapped with the second peak is possibly due to a typical transition of unintentionally doped Mn^{2+} ions. The peak around 580 nm is higher by a relatively large extent when the phosphor layer is doped with 0.1 mol % of Pr and Ce as compared to the case of 0.3 mol % doping. This fact can be explained by assuming the nonradiative energy transfer from the $5d(^2D)-4f(^2F_{5/2})$ transition of Ce^{3+} ions to unidentified defects which are no longer present below 0.3 mol % of Ce and Pr. If the excess doping of Ce above 0.3 mol % is performed, a nonradiative energy transfer to the various defects with a large resonant absorption for the $5d(^2D)-4f(^2F_{5/2})$ emission of Ce^{3+} is possible due to lattice distortion mostly induced by the excess doping with two different valence ions (Pr^{3+} and Ce^{3+}) substituting for the Zn^{2+}. In this case, it seems that the unintentionally incorporated Mn^{2+} ions,[5] which are detected by electron paramegetic resonance (EPR) experiments in the ZnS:Pr,Ce,F layer, may reduce the native defect density, leading to a better stoichiometry as well as better charge compensation as previously shown in crystallinity and luminescence results. The obtained EL emission spectrum of ZnS:Pr(0.1), Ce(0.1),F satisfy approximately the complementary color relationship, resulting in a nearly paperlike white emission. On the other hand, the effect of Mn ions on the emission characteristics of the ZnS:Pr,Ce,F phosphor will be discussed in another article.

The x-ray photoelectron spectroscopy results suggest that the decrease of intensity in the region of 525–550 nm, which appears in the ZnS:Pr(0.3), Ce(0.3),F, is thought be a phenomena related to oxygen since the layer has partial SO_4 and SO_3 bonds. Since the excited states of Ce^{3+} ions are not shielded by the $5S^25P^6$ closed shells, the states are easily affected by the crystal field distortion of the Pr(0.3) and Ce(0.3) doubly doped ZnS host[6] and therefore the transition was changed.

In order to investigate the mechanism of electroluminescence of our ZnS:Pr,Ce,F device, we measured the light emission wave form and conduction current wave form using the modified Chen–Krupka circuits under the excitation of triangular wave form. Figure 8 shows the temporal responses of EL emission and the current of our EL device under high voltage excitation. Only one emission peak is observed at the peak of the excitation voltage despite containing two different emission centers.

In conduction current wave form a steplike form is observed, as shown in Fig. 8. This form indicates that the conductive current flows in addition to the capacitive current. The decay curves for selected emissions of ZnS:Pr(0.8 mol %),F, ZnS:Pr(0.1),Ce(0.1),F, and ZnS:Pr(0.3),Ce(0.3),F films are plotted from the top, respectively, in Figs. 9(a), 9(b), and 9(c). The decay time constant τ corresponding to each emission is estimated by the time at which the maximum intensity has decreased by a factor of e^{-1}. The time

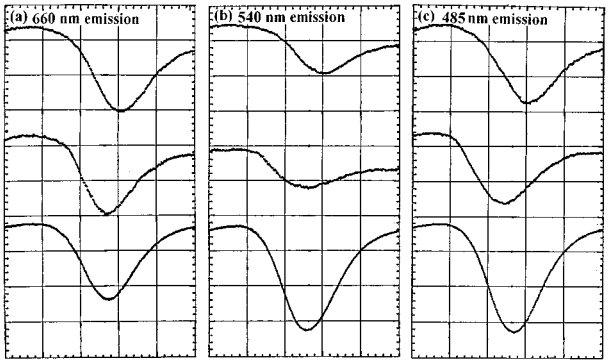

FIG. 9. The decay wave forms of light emissions of EL devices corresponding to (a) 660 nm emission, (b) 540 nm emission, and (c) 485 nm emission of ZnS:Pr(0.8mol %), F, ZnS:Pr(0.1mol %), Ce(0.1mol %), F, and ZnS:Pr(0.3mol %), Ce(0.3mol %), F from top to bottom, respectively.

constant of 540 nm emission, τ_{540} ZnS:Pr(0.8),F EL device, is shorter than τ_{485}. In the case of the ZnS:Pr(0.1),Ce(0.1),F EL device, τ_{540} is larger than τ_{485}. However, the ZnS:Pr(0.3),Ce(0.3),F EL device shows that τ_{540} is nearly equal to τ_{485}. This fact implies that 540 nm emission decays more rapidly in ZnS:Pr(0.8), F via an unknown nonradiative defect, than 485 nm emission. Since the decay time depends on the surrounding nonradiative defects, these results indicate that an appropriate Ce (and Mn) codoping can reduce the nonradiative energy transfer via unidentified defects in both emissions, particularly in the 540 nm emission to a large extent. The results also imply that new types of nonradiative defects are created when the total doping concentration of Pr and Ce reaches 0.3 mol % or higher. Therefore, it is certain that the codoping of Ce with optimum concentration results in a decreased concentration of the unidentified defects as compared to single Pr (0.8 mol %) high doping. Here, we suggest that the possible defects are Pr–Pr pairs or clusters in a singlely Pr-doped ZnS layer and Pr–Ce pairs or defects due to uncompensated valency in the ZnS:Pr,Ce,F lattice, since the decrease of concentration of Pr ions from 0.8 mol % to 0.1–0.3 mol % results in an increase of decay time and excess Ce codoping beyond 0.3mol % resulted in a similar decrease of decay time as observed in the ZnS:Pr(0.8mol %),F EL device.

Similar to the results of the ZnS:Pr,F EL device,[3] the occurrence of the maximum emission nearly coincides with the peak of the conductive current in the ZnS:Pr(0.1),Ce(0.1),F EL device. It implies that the dominant emission process of the latter is the impact excitation of Pr. On the other hand, the ZnS:Pr(0.3),Ce(0.3),F EL device shows very different phenomena such that the maximum emission occurs after the peak of the applied voltage. This fact suggests that the EL mechanism of the ZnS:Pr(0.3),Ce(0.3),F EL device is different from the other two types of EL device.

B. Role of the interlayer on the operating characteristics of the EL device

1. Breakdown characteristics of the EL device with and without an interlayer

Many works have been reported on the method of improving the luminous efficiency and the aging characteristics

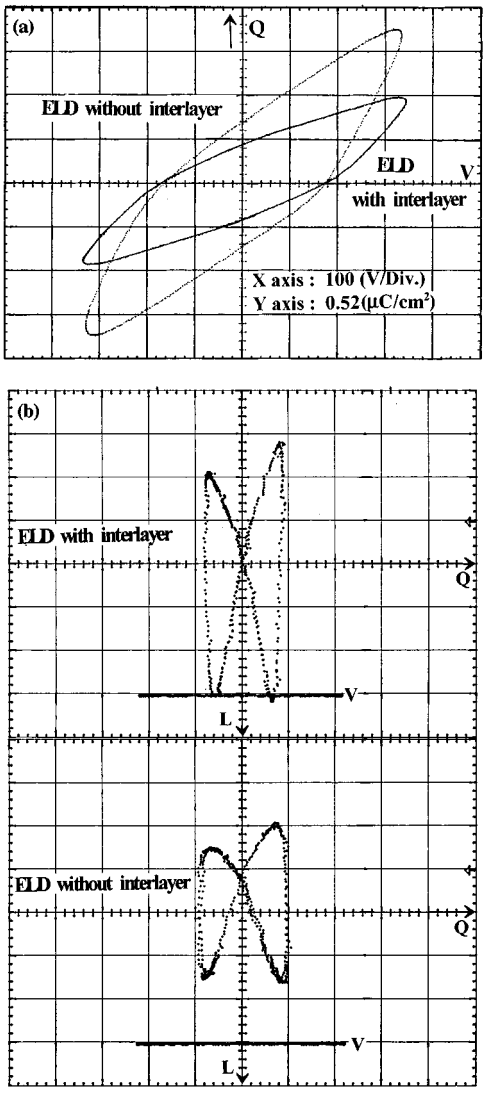

FIG. 10. (a) Transferred charge (Q) vs applied voltage loops and (b) luminance vs transferred charge loops of EL devices.

of the EL device, but most of them have been concerned with improving device fabrication techniques to enhance the excitation efficiency by increasing the electron mean-free path within the phosphor layer. Alternatively, an increase in the internal electric field would provide an enhancement of efficiency, but is limited to a very small range, since the clamping field of a typical thin film device is just slightly above the threshold field of the EL device operation, i.e., $2-3\times10^6$ V/cm.[7] In essence, it has been concluded that any improvements in efficiency are restricted by the optimization of fabrication techniques, and are therefore limited due to this field clamping effect.[8] In this section we present and discuss results which were obtained from a study of a simple method of improving efficiency and degradation characteristics of a ZnS:Pr(0.1),Ce(0.1),F EL device, by controlling the electron conduction process.

Transferred charge versus applied voltage ($Q-V$) diagrams of the devices with and without an interlayer are also shown in Fig. 10(a), and the transferred charge versus luminance ($L-V$) loops of both devices are shown in Fig. 10(b).

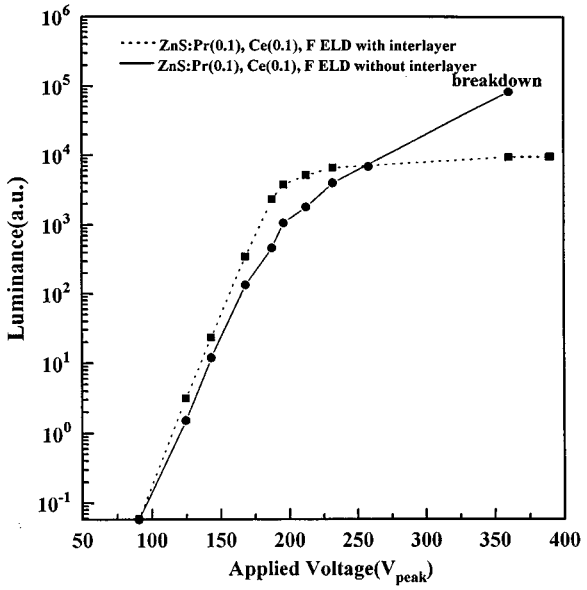

FIG. 11. Luminance vs applied voltage characteristics of an EL device with an interlayer (rectangular symbol) and without an interlayer (circle symbol).

The threshold voltage V_{th}, the required voltage to obtain a brightness of 1 cd/m^2, was approximately 115 and 125 V for EL devices with and without an interlayer, respectively. The $L-V$ curves commonly show steep slopes and the failure breakdown voltage of the TFEL device was found to be greater than 360 V. The $Q-V$ diagrams of Fig. 10(a) were measured with 320 V excitation, when the EL device exhibits strong emission. From the $Q-V$ analysis, it was clarified that the maximum charge storage capacity of both devices is determined by the $BaTa_2O_6$ insulating layer. If the thin interlayer determines the maximum charge storage capacity of the device, the device must break down in the region around 0.5–1 μC/cm^2 of the charge storage capacity of our interlayer. Result indicates that the thin interlayer does not exhibit destructive breakdown but experiences dielectric avalanche breakdown in the region above its own breakdown field under current condition. Therefore, the breakdown voltage related to the stability of the EL device is not determined by the thin interlayer but by the $BaTa_2O_6$ insulator which has the highest Q_{max} among the device components and the value is equal to the applied voltage at which the electric field in the $BaTa_2O_6$ layer reaches its own breakdown field (Fig. 11).

2. Influence of the thin interlayer on the luminous efficiency

In order to investigate the effect of doping concentration on efficiency as a function of emission wavelength, we have measured the luminance versus transferred charge ($L-Q$) loops. The efficiency in this study is defined as the slope of the $L-Q$ loop, that is dL/dQ,[9] and the obtained results are shown in Figs. 10(b), 12, and 13. For the device with the ZnS:Pr,F phosphor layer, the efficiency is highest at 660 nm, is lower at 540 nm, and is lowest at 485 nm. The ZnS:Pr(0.1), Ce(0.1), F device without an interlayer showed a similar trend to the ZnS:Pr, F device, but the efficiency in the interlayered ZnS:Pr(0.1), Ce(0.1),F device is at a maximum at 485 nm, is lower at 540 nm, and is lowest at 660 nm as shown in Fig. 12(a). Thus, we can conclude that the energy distribution of the transported electrons is shifted to the higher energy in the interlayered EL device, and such a stronger excitation at a short wavelength is preferable for the color EL devices.

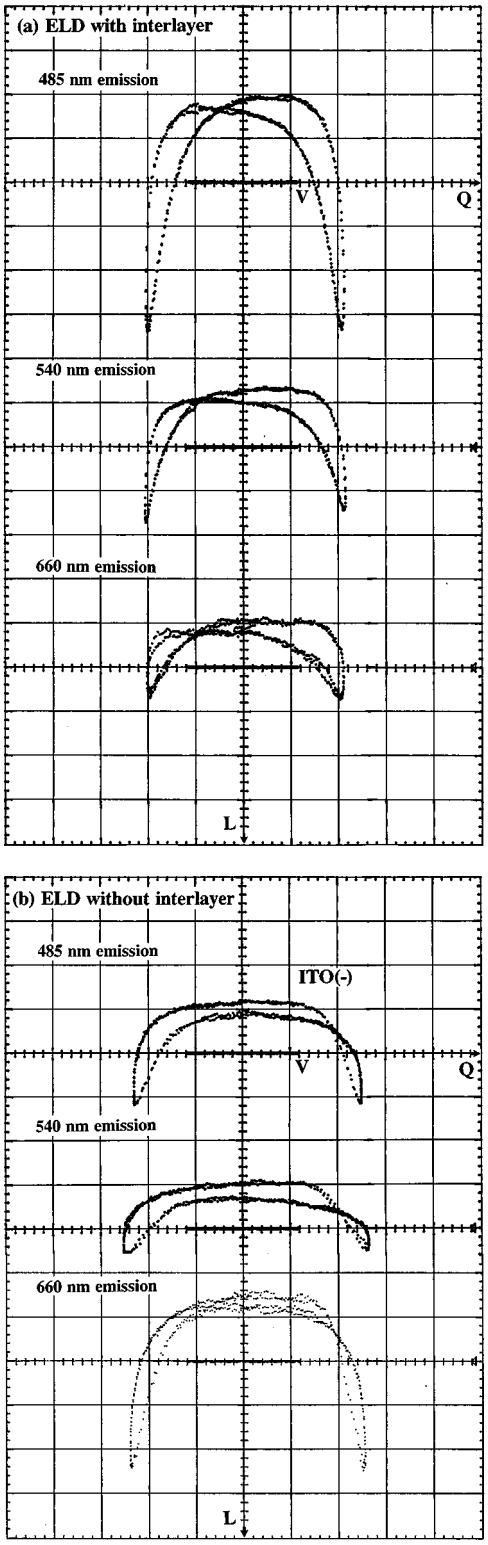

FIG. 12. Luminance vs transferred charge (Q) loops as a function of emission wavelength of an EL device (a) with an interlayer and (b) without an interlayer.

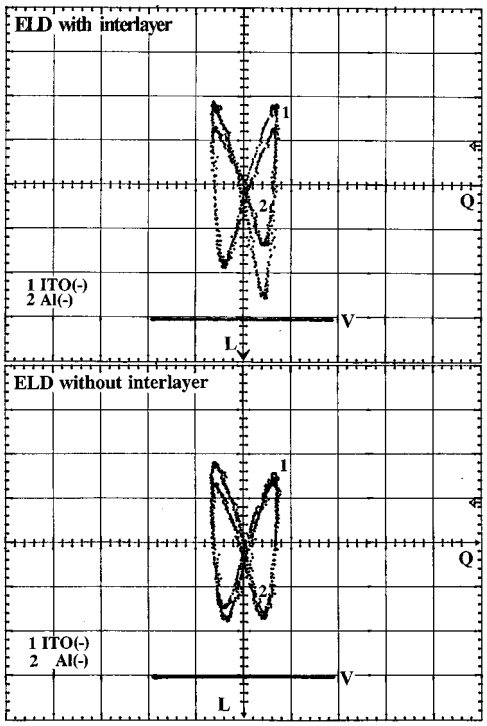

FIG. 13. Light output vs transferred charge loops of the direct view luminous efficiency as a function of the applied polarity of the voltage: (a) an EL device with an interlayer, (b) EL device without an interlayer.

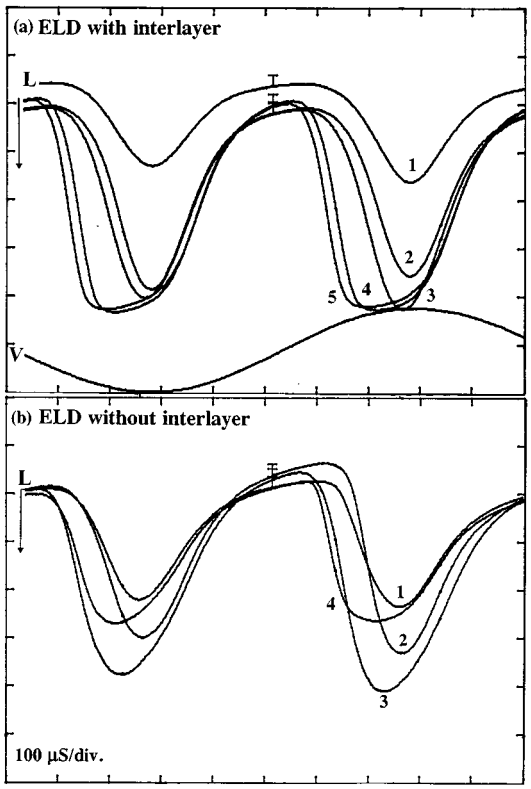

FIG. 14. Light emission wave forms at several different excitation voltage levels: (a) an EL device with an interlayer, (b) an EL device without an interlayer.

The emission symmetry as a function of the polarity of the applied voltage measured with a sine wave form of 1 kHz is shown in Fig. 13. The luminance versus transferred charge ($L-Q$) loop of the EL device, without an interlayer showed nearly the same emission intensities when changing the polarity, although the efficiency was slightly higher when the negative voltage was applied to the ITO side. But for the EL device with a thin Si_xN_y interlayer between the lower insulator and the phosphor layer, the asymmetry of luminous efficiency was further increased and the intensity ratio of the emission at different polarities was in the range from ~0.6 to 0.9. The luminous efficiency and the emission intensity under the same transferred charge were larger when electrons flowed through the upper $BaTa_2O_6$ to the ZnS:Pr,Ce/Si_xN_y/lower $BaTa_2O_6$ interface by applying negative voltage to the ITO side. The aging characteristics of EL devices with and without an interlayer were very different from each other. The initial luminous efficiency of the EL device without an interlayer was superior to that with an interlayer, but the efficiency was rapidly decreased. The better stability of luminous efficiency of the interlayered interface implies a change in the properties of the $BaTa_2O_6$/ZnS:Pr, Ce, F interface with the insertion of 50-nm-thick Si_xN_y interlayer. Thus the insertion of an interlayer not only enhances the asymmetric luminous characteristics of the lower interface, but also simultaneously maintains excellent charge storage capacity during EL emission.

We next discuss the various characteristics of our device in order to understand the effect of an interlayer on the luminous efficiency. The increase of luminous efficiency in the interlayered device was always accompanied by a reduction in the transferred charge, which was confirmed by the previous $Q-V$ and $L-Q$ measurements.

In a separate experiment,[10] we found that the transferred charge of EL devices with an interlayer was nearly independent of temperature, which is supposedly some evidence of a typical tunneling process. But in the case of an EL device without an interlayer, the transferred charge increased exponentially with temperature. Therefore, we suggest that one of the conduction process in an EL device without an interlayer is Poole–Frenkel conduction, in which electrons are emitted from the bulk traps. This suggestion was supported by the observation shown in Fig. 14. In case of an EL device without an interlayer, increasing the applied voltage resulted in decreasing emission, while the interlayered EL device showed increasing emission with voltage.

There are two possible roles of a thin insulating interlayer; it generates additional interface states contributing to the primary electrons available for the excitation of light-emitting centers or it acts as a tunneling layer in such a manner that electrons that tunnel through the thin interlayer acquire sufficient energy, thereby increasing the excitation efficiency of light-emitting centers. In the present case, the analysis of the transferred charge characteristics confirmed that the dominant role of the interlayer is as a tunneling barrier since there is a decrease in the transferred charge after insertion and the magnitude of the transferred charge is found to be temperature independent. Therefore, it is possible to modify the electron emission characteristics and the conduction process by inserting an interlayer of 50-nm-thick

silicon nitride in such a way that both the tunneling efficiency of electrons and the excitation efficiency of light-emitting centers are enhanced.

IV. CONCLUSION

In this work we fabricated bright white-light-emitting EL devices with a Pr and Ce doubly doped ZnS phosphor layer. Filtered red, green, and blue spectral components had sufficient luminance for applications to the color EL devices. In order to improve the efficiency and the degradation characteristics of the ZnS:Pr,Ce,F EL device, we fabricated EL devices with and without an interlayer. From the analysis of the transferred charge characteristics as a function of applied voltage and the luminous efficiency characteristics, we confirmed that the dominant role of an interlayer is as a tunneling barrier that enhances the electron conduction process, and thus the excitation efficiency of light-emitting centers.

ACKNOWLEDGMENT

This work was supported by the Ministry of Science and Technology in Korea.

[1] K. Hirao, M. Higuchi, and N. Soga, J. Lumin. **60/61**, 115 (1994).
[2] R. Fukao, H. Fujikawa, and Y. Hamakawa, Jpn. J. Appl. Phys. **28**, 2446 (1989).
[3] Y. H. Lee, B. K. Ju, T. H. Yeom, D. H. Kim, T. S. Hahn, S. H. Choh, and M. H. Oh, J. Appl. Phys. **75**, 1 (1994).
[4] Y. Abe, K. Onisawa, K. Tamura, T. Nakayama, M. Hanazono, and Y. A. Ono, Springer Proc. Phys. **38**, 199 (1989).
[5] Y. H. Lee, D. H. Kim, B. K. Ju, M. H. Song, T. S. Hahn, and M. H. Oh, J. Appl. Phys. **78**, 15 (1995).
[6] R. Mach, G. U. Reinsperger, G. O. Muller, B. Selle, and G. Matzkeit, J. Cryst. Growth **177**, 1002 (1992).
[7] C. B. Thomas and W. M. Cranton, Appl. Phys. Lett. **63**, 3119 (1993).
[8] W. M. Cranton, D. M. Spink, R. Stevens, and C. B. Thomas, Thin Solid Films **226**, 156 (1993).
[9] J. Ohwaki, H. Kozawaguchi, and B. Tsujiyama, J. Electrochem. Soc. **137**, 340 (1990).
[10] M. H. Song, Y. H. Lee, B. K. Ju, T. S. Hahn, and M. H. Oh, J. Cryst. Growth (to be published).